International Journal of Nanomedicine

Dovepress
open access to scientific and medical research

Open Access Full Text Article

ORIGINAL RESEARCH

Platelet-Mimicking Drug Delivery Nanoparticles for Enhanced Chemo-Photothermal Therapy of Breast Cancer

This article was published in the following Dove Press journal:
International Journal of Nanomedicine

Wenjing Pei[1,2]
Biying Huang[1,2]
Sijie Chen[1,2]
Long Wang[3]
Yan Xu[1,2]
Chengcheng Niu[1,2]

[1]Department of Ultrasound Diagnosis, The Second Xiangya Hospital, Central South University, Changsha, Hunan 410011, People's Republic of China; [2]Research Center of Ultrasonography, The Second Xiangya Hospital, Central South University, Changsha, Hunan 410011, People's Republic of China; [3]Department of Orthopedics, Xiangya Hospital, Central South University, Changsha, Hunan 410008, People's Republic of China

Background: Traditional nanoparticle-based drug delivery systems suffer from several limitations, such as easy clearance from blood and inaccurate targeting.

Materials and Methods: Here, we developed platelet membrane-coated nanoparticles (PM-NPs) to improve the precise delivery of drugs to tumor sites and enable a more efficient photothermal therapy (PTT) treatment.

Results: Mimicking the natural platelet membrane, nanoparticles containing drugs and photothermal agents were not recognized and cleared by the immune system; they could circulate in the blood for a long time and accumulate more efficiently at the tumor site, thus releasing more antitumor drugs and achieving better PTT effects. It is worth mentioning that, in this study, we found that tumors in mice treated with the platelet-mimicking nanoparticles were completely eliminated without recurrence during the observation period (up to 18 days).

Conclusion: This study provides a new strategy to design delivery systems of drugs or photothermal agents, whether in biotherapy or other fields.

Keywords: platelet-mimicking, drug delivery, IR780, doxorubicin, chemo-photothermal therapy

Introduction

Breast cancer, a most common malignant tumors in females and seriously harms the life quality and lives of women worldwide.[1] Photothermal therapy (PTT) has drawn widespread attention due to its advantages of noninvasiveness, safety, and good selectivity compared with traditional surgery and chemotherapy.[2,3] The principle of PTT is to focus the laser directly on the tumor site and use its heating ablation to kill tumor cells. Most of the free photothermal therapeutic agents cannot accumulate at the tumor site efficiently due to solubility issues, fast metabolism, or restrictions in their direct administration because of safety considerations. Therefore, nanocarriers have become the first choice of scientists to solve the abovementioned problems. Moreover, tumor accumulation of nanomaterials could be realized through the EPR (enhanced permeability and retention) effect as a result of the nanoscale size. However, biocompatibility and stability of nanoparticles are critical aspects in the design process. To address these issues, the synthetic polymer poly(ethylene glycol) (PEG)[4,5] can be introduced onto the nanoparticle surface. However, PEGylated nanoparticles are still foreign matter to the human body, and

Correspondence: Chengcheng Niu
Department of Ultrasound Diagnosis, The Second Xiangya Hospital, Central South University, Changsha, Hunan 410011, People's Republic of China
Email niuchengcheng@csu.edu.cn

submit your manuscript | www.dovepress.com
DovePress
http://doi.org/10.2147/IJN.S285952

even excellent nanoparticles with good biocompatibility still face the problem of being eliminated by the immune system. Therefore, avoiding the quick clearance by the immune system is a key performance factor. Scientists have also tried to use targeting ligand conjugation strategies. However, this process is difficult and not suitable for large-scale manufacturing,[6] and it may result in new problems. Natural microscopic carriers in human body-active cells, such as RBCs, PLTs, and WBCs, have efficient circulation capabilities and a variety of physiological functions in the body. The application of these natural materials to nanomedicine could easily, economically, and effectively eliminate the immunogenicity of nanoparticles and address their limitations, such as poor aggregation at the tumor site caused by rapid clearance, and other side effects.

The design approaches of biomimetic nanoparticles have recently emerged as a novel paradigm.[6] Since Zhang's team used erythrocyte membranes wrapped around nanoparticles for the first time to improve the biocompatibility of nanomaterials,[7] researchers have dedicated much effort to find more applications of biomimetic nanomaterials in the treatment of various diseases.[8–15] Various cell types have been developed, including macrophages,[16–18] T cells,[19,20] neutrophils,[21,22] stem cells,[23–27] red blood cells,[28–32] and platelets.[33,34] Biomimetic nanomaterials show many advantages, such as high biocompatibility, longer cycle life, inherent biodegradability, natural targeting ability of cells/tissues, high drug loading, and ability to cross biological barriers. Considering the various benefits of bionic nanomaterials compared with traditional nanoparticles, this biomimetic technology has great prospects in the future. In particular, platelets participate in many important physiological functions, hemostasis, immune escape,[35] subendothelial adhesion,[36] and pathogen interaction,[37,38] and play an significant role in tumor metastasis.[39] Therefore, coating natural platelet membranes onto nanoparticles has provided a new approach for nanocarrier design, which can be applied various biomedical fields.

Here, we designed platelet membrane-wrapped PLGA nanoparticles loaded with chemotherapeutic drugs and photothermal agents for combined chemotherapy and PTT. We illustrated the successful preparation process of these platelet membrane-coated IR780@PLGA/Dox (PM-NPs). This method is simple and time-saving, which is convenient for future clinical use. We chose the typical near-infrared (NIR) fluorescent dye IR780 as the photothermal agent due to its tumor-targeting capability[40] and excellent optical properties. But IR780 has many limitations to be applied in vivo such as poor water solubility, toxicity, and fast clearance,[41,42] so we adopted PLGA, a polymer material with good biocompatibility to load IR780. The tissue penetration depth of laser irradiation is sometimes not enough to eliminate tumors thoroughly, so chemotherapy was also designed in this study to improve antitumor efficacy. Doxorubicin hydrochloride (Dox) as the therapeutic chemotherapy drug was wrapped in the core of PM-NPs. We evaluated the ability of the PM-NPs to release drugs in two pH environments and the uptake of the PM-NPs by two relevant cell lines in vitro. In vivo fluorescence imaging was used to investigate the biodistribution and targeting ability after intravenous injection, and related pharmacokinetic studies were performed. Finally, we evaluated the antitumor efficacy and biosafety of the PM-NPs in 4T1 tumor-bearing Balb/c mice. The results manifested under the premise of safety, the nanoparticles exhibited a longer circulation time in the body, strong tumor targeting ability, and enhanced antitumor efficacy.

Materials and Methods

Materials

Poly (lactic-co-glycolic acid) (PLGA), IR780 iodide, and polyvinyl alcohol (PVA) were all obtained from Sigma-Aldrich (USA). Doxorubicin hydrochloride (Dox) was purchased from Solarbio Co., Ltd. (China). Both DiI stain kit and BCA protein assay kit were purchased from Beyotime Inst. Biotech (China). The platelet protein extraction kit was purchased from BesBio (China). The Calcein-AM/PI Double Stain Kit was obtained from Yeasen (China). The Cell Counting Kit-8 (CCK-8) was obtained from 7sea Biotech (China). All experiments were approved by the Ethics Committee of the Second Xiangya Hospital, Central South University, China.

Isolation of Platelets and Preparation of Platelet Membranes

Whole blood was obtained from male KM mice by puncture of the submandibular vein with an Eppendorf tube coated with ethylenediaminetetraacetic acid (EDTA) in the inner layer. The platelets were isolated and the PM membrane was obtained by using the previously reported method,[43] the specific preparation process is detailed in Supporting information.

Synthesis of IR780@PLGA/DOX NPs

The nanoparticle cores were prepared via a single emulsification method. Two hundred milligrams of PLGA was dissolved in 6 mL dichloromethane. After fully dissolving, 6 mg IR780, 0.2 mL of a DOX solution (with a Dox concentration of 20 mg/mL) and 30 mL of a 4% (w/v) PVA solution were put into the above system. Then, the mixture was emulsified with an ultrasonic processor on ice for 2 minutes, 40 mL of deionized water was added, and the mixture was stirred for 2 ~ 4 h and washed with deionized water for at least 3 times. The whole procedure was kept from light. The final output was kept at 4°C in dark place.

Preparation and Characterization of PM-NPs

To coat the platelet membranes onto the IR780@PLGA/DOX NPs (designated NPs) surface, 1 mL of water containing 2 mg of NPs was mixed with platelets vesicles which were obtained from 1 mL of mice whole blood. The above mixture was then sonicated for 5 minutes in the dark and centrifuged at 14,000 × g to remove excess PLT vesicles. Then, precipitation was resuspended with PBS and preserved at 4°C and avoid light for further use. The size distributions and zeta potentials of the NPs and the PM-NPs were measured with a zetasizer (Nano ZS, Malvern). The morphologies were observed by a TEM (G2 F20 S-TWIN, Tecnai) operating at 120 kV after staining with 2% (w/v) uranyl acetate. UV-vis spectra were recorded with a microplate reader (Spectra Max M2/M2e).

To study the protein components in the PM-NPs, Western Blot was employed. We extracted the proteins from the freshly extracted platelets, platelet vesicles, and the PM-NPs with a protein extraction kit (Best bio), and then samples were normalized to the equal protein concentration with a BCA assay (Beyotime). Then, the following steps were completed by a known procedure and developed with ECL substrate.

Drug Loading, Encapsulation and Release Characterization

The prepared PM-NPs were centrifuged, and the precipitate was preserved. To test the IR780 loading capability of the PM-NPs, the precipitate was dried for 24 h using a vacuum freeze dryer. Then, the freeze-dried PM-NPs were dissolved in 1 mL of DMSO and diluted, and the absorbance of IR780 at 791 nm was detected by UV-Vis-NIR spectrophotometer. The IR780 encapsulation efficiency and loading efficiency were calculated according to (1) and (2) as follows:

$$\text{Encapsulation efficiency (\%)} = W_E/W_T \times 100\% \quad (1)$$

$$\text{Loading efficiency (\%)} = W_E/W_N \times 100\% \quad (2)$$

W_E refers to the amount of IR780 encapsulated in the NPs, W_T refers to the total amount of IR780 added, and W_N refers to the dry weight of the NPs.

To evaluate the Dox loading capability of the PM-NPs, they were dissolved in solvent (water: DMSO=1:9) and sonicated for 30 minutes. Afterwards, we measured the fluorescence intensity at 596 nm (Ex of Dox: 480 nm). A standard curve was obtained using the same solvent. The encapsulation efficiency and loading efficiency of Dox could be acquired with the same method mentioned above.

To investigate Dox release under different pH conditions, 0.2 mL of NPs or PM-NPs was added to a dialysis bag, with or without laser irradiation (808 nm, 1 W/cm^2, 5 min), and then submerged in PBS of 20 mL at different pH environment (5.0 or 7.4) in a dark container and gently vibrated in a shaker (BSD-TX345, Shanghai Boxun) at 100 rpm. At predesignated time intervals, 0.2 mL of the solution was removed from the container and replaced with 0.2 mL of fresh PBS with the same pH. Then, the fluorescence intensity at 596nm was measured immediately.

In vitro Photothermal Effects of PM-NPs

PBS, Dox, platelet vesicles, NPs, and PM-NPs were dispersed in deionized water in eppendorf tubes separately and irradiated for 5 minutes by an 808 nm laser (T808F2W, Minghui Optoelectronic Technology, China) (1 W/cm^2). The temperatures were then recorded every specific time points by an infrared thermal imager (FLIR C2, USA).

In vitro Stability Study of PM-NPs

To access the stability of the nanoparticles, the experiments were conducted by measuring the DLS diameters of the NPs and PM-NPs in 10% FBS (HyClone) at 37°C every 24 h for 7 days.

Cell Culture

4T1 mouse breast cancer cells and Raw 264.7 cells were purchased from the China Center for Type Culture Collection (Wuhan, China) and cultured in RPMI (1640) medium or Dulbecco's Modified Eagle Medium (DMEM) containing 10% (v/v) fetal bovine serum and 1% (v/v) penicillin-streptomycin.

Intracellular Uptake

4T1 cells (1×10^4 cells/well) and Raw 264.7 cells (1×10^5 cells/well) were seeded on 6-well plates. After 24 h, DiI-labeled NPs or PM-NPs were separately added to fresh serum-free medium and incubated for 0.5, 2, and 4 h. Then, the cells were gently washed using cold PBS for three times in the dark, then fixed with 4% paraformaldehyde and stained with DAPI. Afterwards, the cells were observed with an inverted fluorescence microscope. The gray value of images with red fluorescence was analyzed by ImageJ. For quantitative analysis, the 4T1 cells incubated with NPs or PM-NPs for 4 h were subjected to flow cytometry for fluorescence signals quantification.

Cell Viability Assay

A 96-well plate was seeded with 4T1 cells (5×10^3 cells/well) and cultured for 24 h. Treatments including free Dox, NPs or PM-NPs (with Dox concentrations of 50, 100, 250, 500, 1000, and 2000 ng/mL) were given and cells were incubated for 24 h. Afterwards, the cells treated with PBS, NPs or PM-NPs at a Dox concentration of 100 or 500 ng/mL were given or not given a 808nm laser irradiation for 5 minutes at 1 W/cm^2. In addition, untreated cells and wells without cells (blank) were used as controls. Three tests were performed per group. After that, in addition to the blank control wells, add 10μL CCK-8 solution to each well and incubate for 3 hours. The OD value at 450 nm was then read by a microplate reader (SpectraMax M2e). The cell viability (%) could be calculated by OD treatment/OD control × 100%.

Apoptosis Assay

Apoptosis of 4T1 cells was detected using the Annexin V-APC/PI Apoptosis Detection Kit (BestBio). 4T1 cells were seeded in the 6-well plates at the density of 1×10^5 cells/well. After culture for 48 h, the cells were treated with PBS, Dox, NPs, and PM-NPs for 2 h (Dox concentration of 500 ng/mL), with or without a NIR laser irradiation (808nm, 1 W/cm^2, 5 min). The subsequent procedures were performed according to the manufacturer's protocol. For Annexin V-APC/PI apoptosis detection, the cells were analyzed by flow cytometry. Furthermore, to visualize the therapeutic effect, the living cells and dead cells were stained with Calcein-AM/PI double staining kit for fluorescence microscope observation.

Animal Models

BALB/c mice, aged 4–6 weeks (female), and KM mice, weighed 34–36 g (male), were both provided by Hunan Silaike Jinda Laboratory Animal Co., Ltd. (China). 4T1 breast tumor-bearing mice were prepared by injecting 100 μL serum-free cell medium containing 1×10^6 4T1 cells subcutaneously into the right flank of BALB/c mice. All animal experiments were approved by the Ethics Committee of the Second Xiangya Hospital of Central South University and conducted in accordance with the guidelines of the Department of Laboratory Animals of Central South University.

In vivo Pharmacokinetics Investigation

The in vivo pharmacokinetics of the nanoparticles were investigated using KM male mice (35 ± 2 g). Ten healthy KM mice were grouped randomly (n=5), then administrated intravenously with the NPs or PM-NPs (0.7 mg/kg of IR780). At present time intervals (0.25, 0.5, 1, 3, 6, 8, 24, 48, 72, 96, 120, 144, 168, 192, and 216 h), blood samples were collected by piercing the submandibular vein with an Eppendorf tube, whose inner surface was coated with ethylenediaminetetraacetic acid (EDTA). The collected blood samples were centrifuged with a speed of 3000 rpm for 10 min. The supernatant was then analyzed by measuring the UV absorbance intensity of IR780.

In vivo Tumor Targeting and Biodistribution Research

Prior to imaging, 30 tumor-bearing BALB/c mice (n=5) were injected with 0.2 mL of NPs or PM-NPs via the tail vein (12, 24, 48, 96, 120 h before imaging) when the tumor volume grew to 200 mm^3. In vivo fluorescent imaging was carried out with IR780 as the fluorescent imaging agent (Ex: 745 nm, Em: 840 nm) by a Lumina IVIS Spectrum imaging system (PerkinElmer, USA). BALB/c mice administrated with PBS only were set blank controls. Mice of each group were sacrificed after the whole-body imaging, and their organs were taken out for in vitro imaging. The average fluorescence intensity of the region of interest (ROI) was further analyzed by Ling image. To evaluate the ability of NPs and PM-NPs to reach the tumor site, 10 tumor-bearing mice (n=5) were injected via the tail vein with DiI-labeled PLGA nanoparticles with or without PM membrane coating separately after the tumor volume reached 200 mm^3. After 48 h, the mice were sacrificed, and the tumor issues were removed and embedded in Tissue-Tek OCT Compound (SAKURA) for frozen sectioning. DAPI was used for nuclear staining, and the tumor slices were imaged with an inverted fluorescence

microscope. To further investigate the Dox distribution at tumor site, the above experiment was repeated, but NPs and PM-NPs without DiI-labeled were administrated instead.

In vivo Combined Chemo-Photothermal Therapy

Mice bearing 4T1 tumors were assigned to six groups (n=10): (1) saline, (2) saline +laser, (3) Dox (Dox of 2.0 mg/kg), (4) PM-NPs only (Dox of 2.0 mg/kg, IR780 of 3.06 mg/kg), (5) NPs +laser (Dox of 2.0 mg/kg, IR780 of 3.06 mg/kg), (6) PM-NPs +laser (Dox of 2.0 mg/kg, IR780 of 3.06 mg/kg). When the tumor volume grew to 100 mm^3, different solutions were injected via tail vein. Twenty-four hours after the injection, the tumor sites of groups (2), (5), and (6) were exposed to an 808 nm laser (1.0 W/cm^2, 5 min). The temperature and infrared images of mice were measured. Tumor size and body weight were recorded every 2 days for 18 days. Photographs of the tumor sites were taken every day to monitor the therapeutic effect of the treatments on those tumors. The mice were killed at the end of observation, and the tumors were removed for H&E, Ki67, and TUNEL staining. The heart, liver, spleen, lung, kidney, and brain were further observed by H&E staining to using an optical microscope.

Statistical Analysis

All data were presented as the mean ± SD. Data analyses were conducted using Origin 2018 software. *$p < 0.05$, **$p < 0.01$, and ***$p < 0.001$ suggests statistically the significant difference.

Results and Discussion

Preparation and Characterization of the PM-NPs

Here, we describe the development of the PM-NPs for improved comprehensive treatment combined with PTT and chemotherapy (Figure 1). The PM-NPs were successfully prepared in the light of a previously reported method.[44] (Figure 1A, Figure S1 and S2, Supporting Information). The preparation process of the PM-NPs is shown in Figure 1. As shown in Figure 1B, the PM-NPs are composed of two components: 1) the PLGA nanoparticle shell was modified with the photothermal agent IR780, and the core was loaded with the small molecular drug Dox; 2) the platelet membranes were coated onto the outer shell to protect the core nanoparticles. The core IR780@PLGA/DOX NPs were prepared on the basis of our previously reported method.[45] The PMs were derived from mouse platelets to coat the surface of the NP core. The PM coating on the NPs can induce multiple functions, such as prolonged blood circulation time, reduced immunogenicity, and more precise tumor targeting.[6] Thus, we hypothesized that this design would increase the aggregation of nanoparticles at tumor site, improving the efficacy of the comprehensive treatment. To demonstrate our hypothesis, IR780 was introduced as a highly efficient photothermal agent on the surface of the nanoparticles to kill the cancer cells via photothermal effects, while Dox was loaded into the PM-NPs as an anticancer therapeutic, which functions by intercalating the nuclear DNA of tumor cells to trigger endogenous apoptosis signaling pathway (Figure 1C).

TEM was used to visualize platelet vesicles (Figure 2A) and the PM-NPs (Figure 2B). The PM-NPs had a smooth, spherical appearance, and the shell thickness of the PM-NPs was approximately 27 nm. The presence of CD47 and CD41,[46] which are specific platelet membrane translocation proteins, was confirmed via Western blotting (Figure 2C), suggesting that the platelet-specific membrane was retained in the PM-NPs. The hydrodynamic size of the IR780@PLGA/DOX NPs was approximately 282.07 ± 4.39 nm and increased to 296.33 ±3.62 nm after PM coating (Figure 2D, Figure S3, Supporting Information). The zeta potential decreased from −1.2475 mV to −22.675 mV with PM coating (Figure 2E), enabling nanoparticles to be more stable in the blood. The increased particle size and decreased surface charge manifested the existence of platelets membrane on the surface of NPs. The UV absorption spectra of PM-NPs with their different components are shown in Figure 2F, indicating IR780 was successfully loaded onto IR780@PLGA/DOX NPs and could act as an excellent photoabsorbing agent;[45] however, the typical absorption peaks could not be observed because Dox was encapsulated inside the nanoparticles, this phenomenon was also found in the previous studies.[45,47]

In vitro Photothermal Performance and Drug Release Characteristics

To study the photothermal effect of the PM-NPs, bare NPs were selected as the control. PBS, Dox, platelet vesicles, NPs, and PM-NPs were exposed to an 808 nm laser for 5 min (1 W/cm^2); the IR780 concentration in both nanoparticles was 3.06 mg/mL. As shown in Figure 3A, PBS as the blank control did not produce a significant temperature increase after laser irradiation, similar to Dox and the

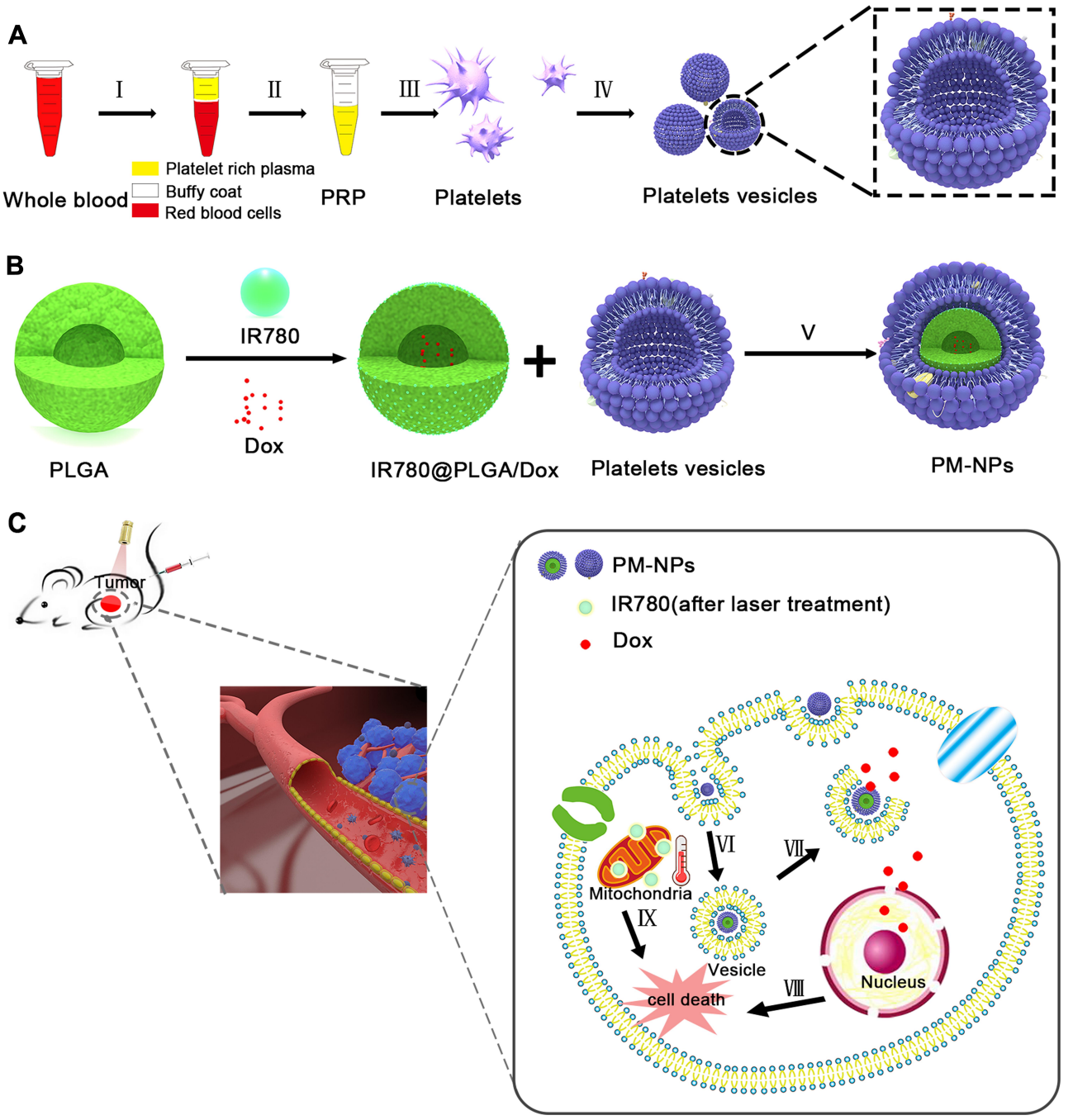

Figure 1 Schematic illustration of the preparation and function of PM-NPs. (**A**) The acquisition process of platelets vesicles. Ⅰ, centrifugation of whole blood; Ⅱ, preservation of the supernatant (PRP); Ⅲ, centrifugation to obtain pure platelets; Ⅳ, repeated freezing and thawing to obtain platelets vesicles. (**B**) The preparation process of PM-NPs. Ⅴ, platelets membrane coating using physical method. (**C**) Mechanism of PM-NPs playing a therapeutic role in killing tumor. VI, endocytosis of PM-NPs by a tumor cell; Ⅶ, the dissociation of PM-NPs; Ⅷ, intrinsic apoptosis triggered by Dox; IX, mitochondrial-targeted IR780 resulted tumor cell death after laser irradiation.

platelets, due to the absence of a photothermal agent. In contrast, the temperature increased notably in the aqueous solutions of the NPs and PM-NPs after laser irradiation, and a temperature change of approximately 30°C was observed for both (Figure 3B). We evaluated the photothermal conversion efficiency by irradiating the NPs and PM-NPs aqueous solutions at a concentration of 4.22 mg/mL (808 nm, 1.0 W/cm^2, 5 min). The linear regression curve of the temperature cooling time (t) vs -ln(θ) of the PM-NPs is shown in Figure 3C. The η values of the NPs and PM-NPs were calculated to be 15.5% and 17.6%, respectively, according to previous reports,[45,47–49] suggesting that the photothermal conversion efficiency of the NPs was retained after PM coating.

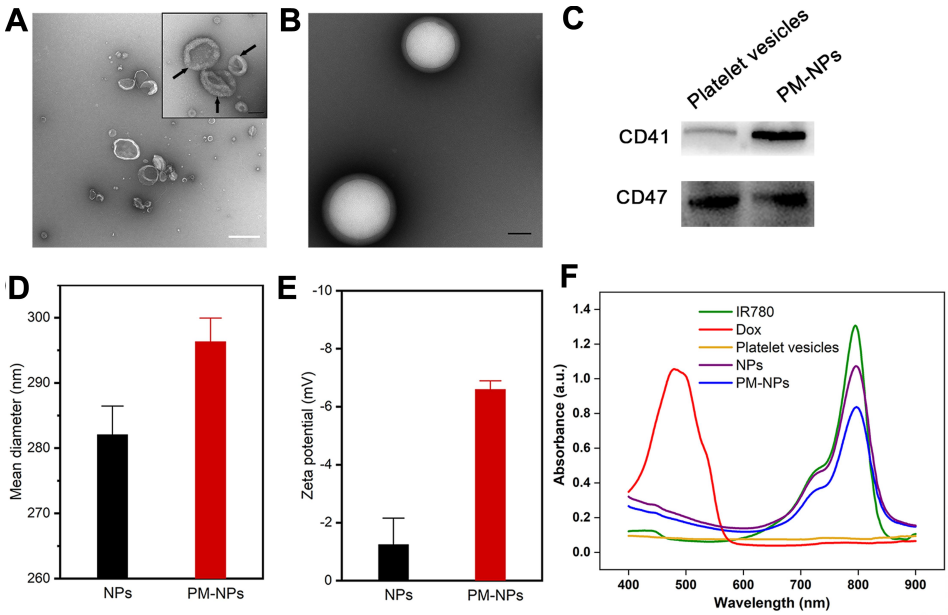

Figure 2 Characterization of PM-NPs. (**A**) The TEM image of platelet vesicles. Scale bar: 500 nm; inset:100 nm. (**B**) The TEM image of PM-NPs. Scale bar: 100 nm. (**C**) Representative CD47 and CD41 protein bands resolved using Western blotting. (**D**) Size and (**E**) zeta potential of NPs and PM-NPs after coating with PM. (**F**) UV–vis–NIR absorption spectra of free IR780, Dox, platelet vesicles, NPs and PM-NPs.

To understand the drug loading properties of the nanoparticles, the encapsulation efficiency (EE) and drug loading (DL) of IR780 (71.26%, 1.69%) and DOX (46.76%, 1.11%) in the nanoparticles were evaluated (Table. S1, Supporting Information). Furthermore, it was important to ensure the structural stability of the nanoparticles before reaching the target tumor site. The size distributions of both nanoparticles stored in 10% FBS at 37°C for 7 days were measured to investigate the colloidal stability. As shown in Figure 3D, there was no significant change in the particle size distribution over time. Therefore, the nanoparticles exhibited good colloidal stability and could be used in subsequent experiments.

To evaluate the Dox release kinetics from the PM-NPs at different pH values, bare IR780@PLGA/DOX NPs were used as the control. The release curve of Dox from the NPs and PM-NPs was obtained at pH 5.0 and 7.4 (Figure 3E and F). Both NPs and PM-NPs released Dox in small amounts at pH 7.4 without laser irradiation (10.38% and 9.11%, respectively, in the first 30 min, 31.86% and 28.90% within 72 h), while the release of DOX increased to 20.88% and 15.97% in the first 30 min, 43.74% and 42.37% within 72 h at pH 5.0. After laser irradiation, the drug release of NPs and PM-NPs increased significantly in both pH environments. Notably, the cumulative Dox release of NPs and PM-NPs reached almost 70% at pH 5.0 at 72 h. The above results indicated that the drug release from our nanoparticles was notably slower at neutral pH values, while the drug release accelerated significantly at the tumor site with acidic pH values. Furthermore, the release rate was extremely accelerated by laser irradiation, resulting in a more efficient targeted release of the antitumor drugs, which may reduce some of the side effects. The prepared NPs and PM-NPs could release more Dox in acidic environments than in neutral environments, and comparing both groups, the release rate of PM-NPs was declined than NPs, suggesting the PM-coating could make the drug release from NPs smoother and longer.

In vitro Cellular Uptake

To understand the in vitro uptake of the nanoparticles by different cells, we added DiI-labeled NPs or PM-NPs to 4T1 or Raw 264.7 cells for 0.5 h, 2 h, and 4 h. Regardless of whether NPs or PM-NPs were used, an obvious red fluorescence was observed, which was attributed to the NPs and PM-NPs accumulated in the 4T1 cells. Furthermore, the intracellular uptake increased over time, and the phagocytic process was basically completed after 2 h (Figure 4). The red fluorescence of the PM-NPs in the 4T1 cells was obviously higher than that of the NPs at each time point,

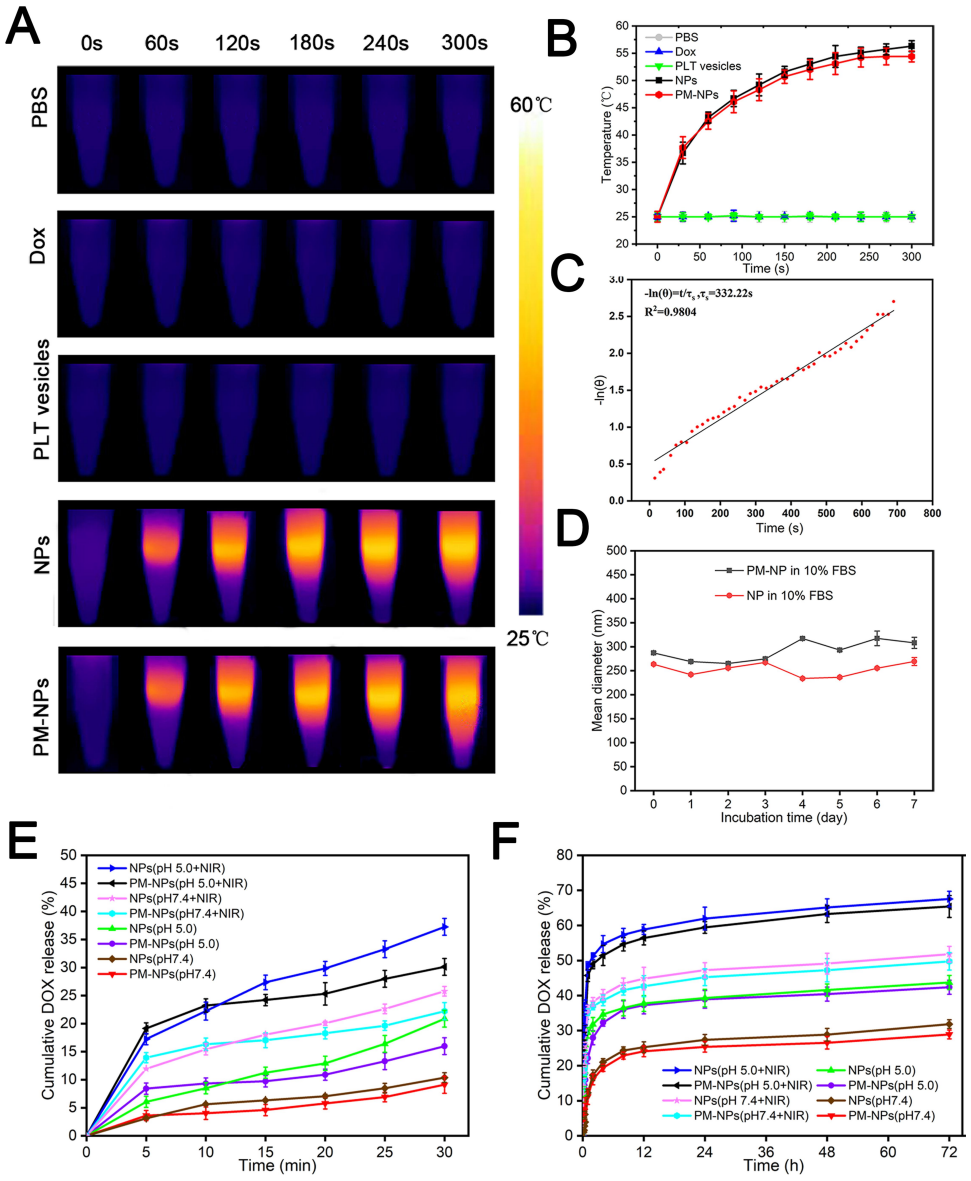

Figure 3 In vitro photothermal effects of PM-NPs. (**A**) Infrared thermal images and (**B**) temperature elevation of PBS, Dox, PLT vesicles, NPs and PM-NPs with laser irradiation (808 nm, 1.0 W/cm^2, 5 min). (**C**) The linear regression curve of temperature cooling time (t) vs -ln(θ) of PM-NPs. (**D**) Size distributions of NPs and PM-NPs in 10% FBS for 7 days. (**E**) After 30 min and (**F**) 72 h, cumulative DOX release from NPs and PM-NPs at pH 5.0 or 7.4 with or without laser irradiation.

indicating that the PM-NPs were more efficiently taken up by the 4T1 tumor cells. As shown in Figure 4D, the fluorescence intensities of 4T1 cells with red fluorescence (DiI) after co-incubation for 4.0 h with two nanoparticles were detected by flow cytometry. The mean fluorescence intensity of PM-NPs was greater than NPs, both of which were significantly higher than the control PBS group. However, more red fluorescence was observed in the RAW 264.7 cells with both the NPs and PM-NPs groups (Figure S4, Supporting Information). Interestingly, the red fluorescence of the PM-NPs in the RAW 264.7 cells was notably lower than that of the NPs, demonstrating that PM-NPs may escape phagocytosis by the reticuloendothelial system (RES) to a certain extent due to the biomimetic properties of the PM coating.

In vitro Antitumor Effect

CCK-8 assays and Calcein/PI staining were used to assess the in vitro antitumor effect of the NPs and PM-NPs. As shown in Figure 5A, Dox, NPs, and PM-NPs (with concentrations of Dox of 50, 100, 200, 500, 1000, and 2000 ng/mL) were added to the 4T1 cells and incubated for 24 h; the cell viability decreased with increasing

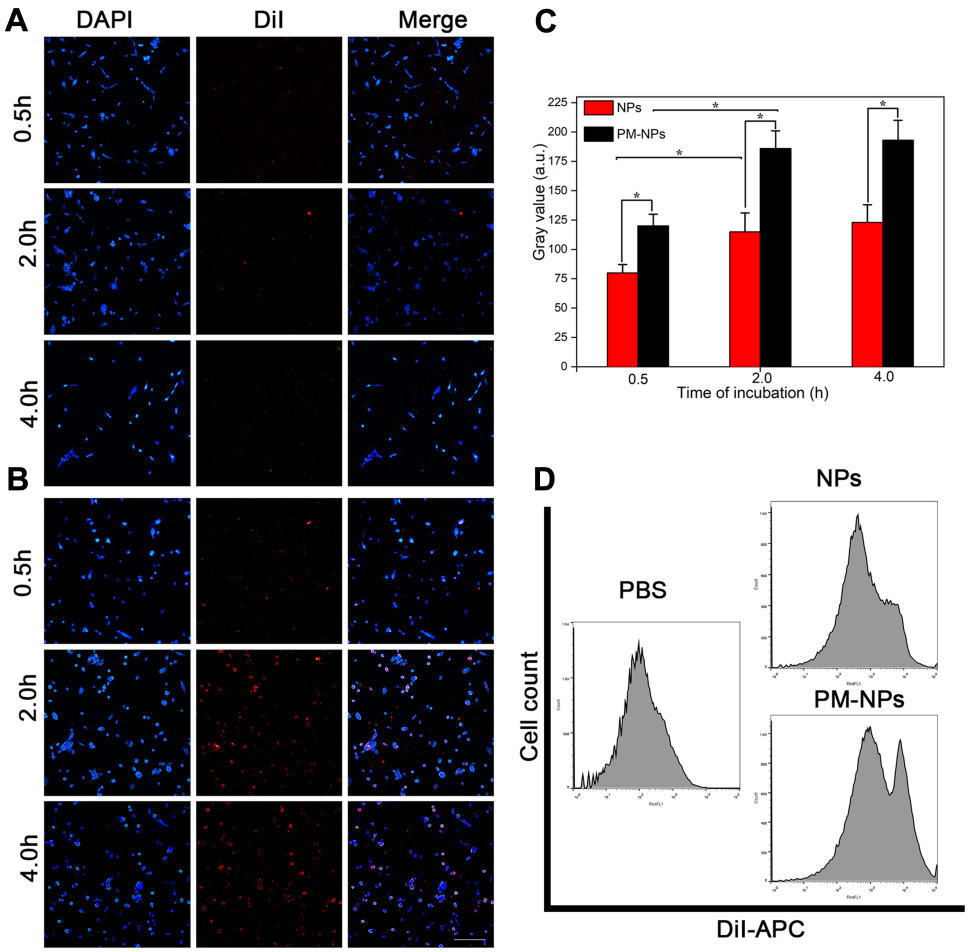

Figure 4 In vitro cellular uptake and intracellular distribution. (**A**) Fluorescence images of 4T1 cells incubated with NPs and (**B**) PM-NPs for 0.5 h, 2 h, and 4 h. Scale bar: 100 μm. (**C**) Corresponding fluorescence intensities of 4T1 cells treated with NPs and PM-NPs for a serious of time (0.5 h, 2.0 h, and 4.0h) (* $p < 0.05$). (**D**) Flow cytometry analysis of 4T1 cells incubated with PBS, DiI-labeled NPs and PM-NPs for 4h.

concentrations of Dox. As shown in Figure 5B, after laser irradiation, the viability of the cells treated with the PBS group showed no obvious difference compared with that group without irradiation, indicating that laser irradiation alone could not kill the 4T1 cells. When the concentration of Dox is 100 ng/mL, the cell viabilities of Dox group with or without irradiation were a little decreased. Both the NPs and PM-NPs groups (Dox concentration of 100 ng/mL) showed an enhanced tumor cell killing effect, suggesting that the NPs and PM-NPs could kill the 4T1 cells via the antitumor effect of Dox and the PTT effect of IR780 during laser irradiation. As the concentration of Dox increased to 500 ng/mL, the tumor cells killing effect was improved further. 4T1 cells were almost killed in PM-NPs group with laser irradiation (Figure 5C).

Then, the tumor killing effect of PM-NPs was observed directly by using calcein/PI staining. The cells were divided into 8 groups: (1) PBS, (2) NIR, (3) Dox, (4) Dox + NIR, (5) NPs, (6) NPs + NIR, (7) PM-NPs, and (8) PM-NPs + NIR. We stained live and dead with calcein (green fluorescence) PI (red fluorescence) separately. As shown in Figure 5D, the 4T1 cells of the control group (1) or NIR group (2), emitted green fluorescence, and only little red fluorescence was observed. After the different treatments, red fluorescence could be observed to different extents. Few dead cells were observed in the Dox group (3), Dox + NIR group (4), NPs group (5) and PM-NPs group (7), while a large number of dead cells were observed in groups containing the NPs (6) or PM-NPs (8) with received laser irradiation, further suggesting that the tumor cells can be effectively killed by our nanoparticles. This result further quantified by flow cytometry (Figure 5E), few apoptotic cells were observed in the Q2 and Q3 area of the control group (1) or NIR group (2), and more than 90% of the cells were located in the Q4 area. The apoptosis rate of 4T1 cells in PM-NPs + NIR group

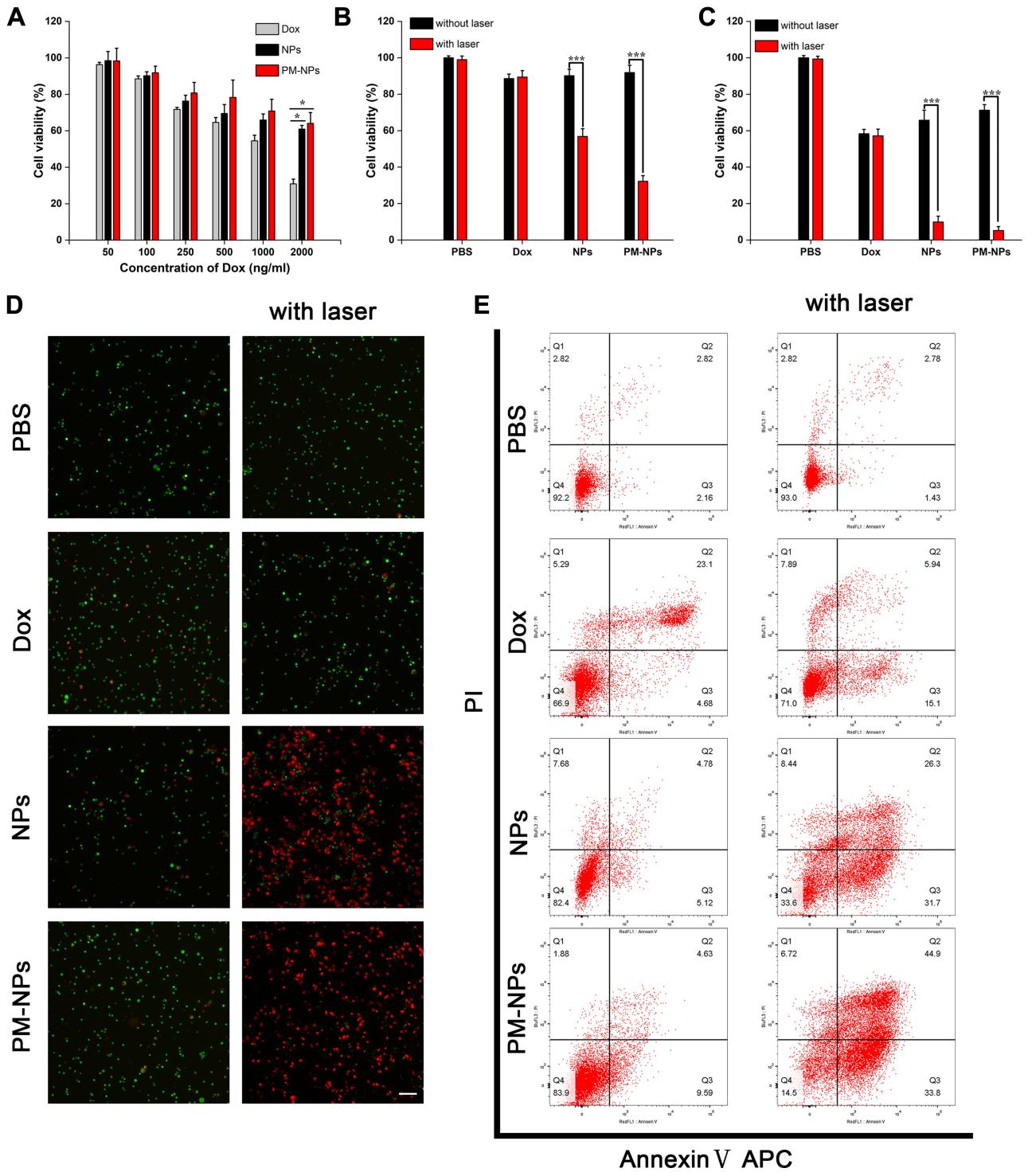

Figure 5 In vitro antitumor effect. (**A**) In vitro cytotoxicity of Dox, NPs, and PM-NPs after incubation for 24 h (* p <0.05). (**B**) Cell viability of 4T1 cells treated with PBS, NPs, and PM-NPs (with 100 ng/mL of Dox) with or without laser irradiation (808 nm, 1.0 W/cm^2, 5 min, ***p< 0.001). (**C**) Cell viability of 4T1 cells treated with PBS, NPs, and PM-NPs with or without laser irradiation (with 500 ng/mL of Dox, *** p <0.001) (**D**) Fluorescence images of 4T1 cells treated with PBS, Dox, NPs, and PM-NPs before and after laser irradiation. Scale bar = 100 μm. (**E**) Flow cytometry: 4T1 cells were treated with PBS, Dox, NPs, and PM-NPs with or without laser irradiation. The Y-axis arrow represents PI, and the X-axis represents Annexin V-APC.

(8) was 78.7%, which was greatly higher than Dox group (3), Dox + NIR group (4), NPs group (5), and PM-NPs (7), and also excellent than NPs + NIR group (6). This demonstrated again the excellent tumor cells killing effect of combined chemo-photothermal therapy, and the binding capacity with tumor cells of PM-NPs to enhance the effect.

In vivo Tumor Targeting Capability of PM-NPs

To assess the pharmacokinetics, the NPs and PM-NPs were administered intravenously, and the concentration of the nanoparticles was obtained by detecting IR780 with a microplate reader. The blood clearance of the PM-NPs seemed slower than that of NPs (Figure S5, Supporting Information). Interestingly, the elimination half-life ($t_{1/2}$) of the NPs was 12.974 h, but that of the PM-NPs was 30.8 h, which was clearly higher than that of the NPs (Table. S2, Supporting Information). Almost 75% of the NPs were cleared from the blood at 72 h, while 43% of the PM-NPs remained in the blood. At the end of the experimental observation, both NPs and PM-NPs were still present in the mouse plasma. The results further confirmed the long-circulation properties of the PM-NPs.

To access the in vivo tumor targeting ability and biodistribution of the PM-NPs, NIR fluorescence imaging was applied. IR780 embedded within the nanoparticles as the photothermal agent, which could also be applied in NIR fluorescence imaging. As shown in Figure 6A, fluorescence could be obviously observed from 12 h to 120 h after injection. The NPs accumulated at the tumor site and showed strong fluorescence, which decreased rapidly. Notably, the fluorescence intensity of the NPs at the tumor site almost disappeared after 120 h. In contrast, the PM-NPs began to aggregate at the tumor site due to their targeting capability and showed a strong fluorescence signal at 24 h, which was maintained at the same intensity for 72 h, after which it declined slightly. As expected, the tumor accumulation of the PM-NPs was enhanced, and longer retention occurred due to the presence of the PM coating. In contrast, the NPs also reached the tumor site due to the targeting ability of IR780,[40] but the fluorescence value decreased immediately after 24 h, indicating that the NPs were metabolized and cleared from the blood. The mice were sacrificed after imaging, and the tumor and other organs were removed for imaging. As shown in Figure 6B and C, the high intensity observed in the lungs may indicate a slow clearance of the nanoparticles by the RES, while a higher accumulation and retention of the PM-NPs at the tumor site at 48 h was observed compared to the uncoated NPs. The results were further verified by a quantitative region-of-interest (ROI) analysis (Figure 6D). As indicated by the histogram, the fluorescence intensity of the PM-NPs group at the tumor site was almost 2-folds higher than that of the NPs group. A high fluorescence intensity was also observed in the lungs due to the enriched RES uptake of IR780-based NPs.[50,51] Besides, another reason for the high lung retention of IR780 may be also related to the particle size, which was nearly 300 nm. Some researchers revealed that the lung retention time was proportional to this particle size.[52] Additionally, the enhanced targeting ability of the PM-NPs was demonstrated by the distribution of the DiI-labeled nanoparticles. As shown in Figure 6E, more red fluorescence signals could be observed in the frozen tumor slices of mice treated with the PM-NPs than in those treated with the NPs.

To further investigate the Dox distribution at tumor site, NPs, and PM-NPs were injected in tumor mice via tail vein, respectively. After 48 h post-injection, the mice tumor tissues were collected and sliced. As shown in Figure S6 in Supporting Information, more red fluorescence signals of Dox could be observed in the frozen tumor slices of mice treated with the PM-NPs than in those treated with the NPs, which further revealed the wonderful enhanced targeting ability of PM coating.

In vivo Tumor-Targeted Combined Therapeutic Efficacy of PM-NPs

To assess the antitumor effect of the PM-NPs, saline solutions of PM-NPs, NPs, and Dox, and saline were injected intravenously into 4T1 tumor-bearing mice. Laser irradiation was performed 24 h after the different treatments (808 nm, 1 W/cm^2, 5 min). The infrared thermal photographs of the mice are shown in Figure 7A. The final temperature of the NPs group reached 56.4°C, whereas that of the PM-NPs group was 56.6°C. The tumor volume and body weight of those mice were observed and recorded every 2 days for 18 days after the intravenous treatment. The growth of the tumor was almost entirely inhibited in the NPs group with laser irradiation (group 5) and the PM-NPs group with laser irradiation (group 6) compared with the saline control (group 1) and the saline group with laser irradiation (group 2) (Figure 7B). The tumor growth of the mice treated with the PM-NPs group without laser irradiation was also inhibited; we therefore assumed that the PM-NPs reached the tumor site, where they released Dox (group 4). However, the PM-NPs could not completely inhibit tumor growth without the effect of thermal ablation, which only has a limited depth. At the end of the experiment, the growth of the 4T1 tumors was completely inhibited in the PM-NPs group with laser irradiation

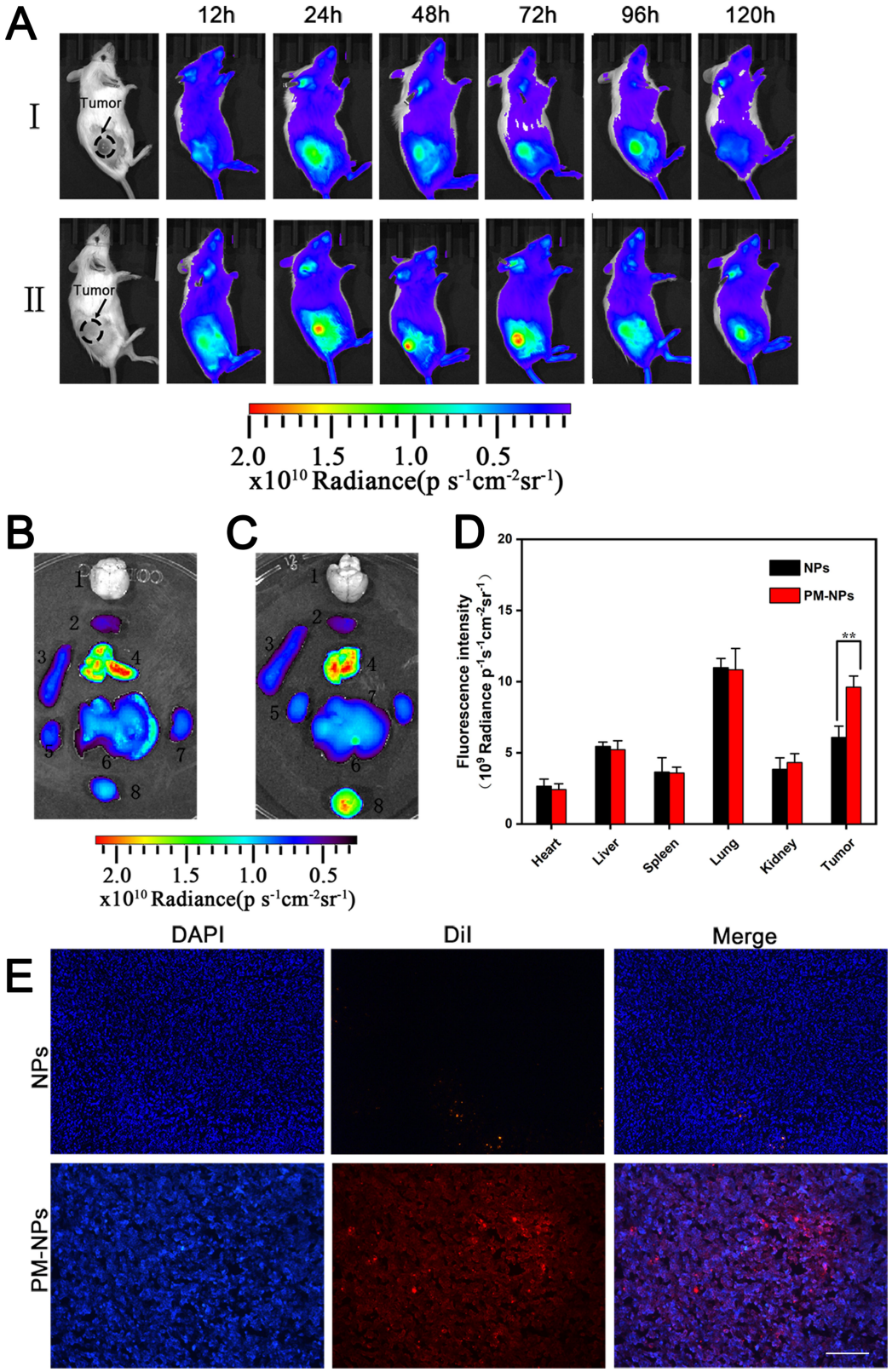

Figure 6 In vivo tumor targeting ability of PM-NPs. (**A**) In vivo fluorescence imaging of 4T1 tumor bearing mice at 12, 24, 48, 72, 96, 120 h after intravenous injection of (Ⅰ) NPs and (Ⅱ) PM-NPs. (**B–C**) Ex vivo fluorescence imaging of major organs and tumors at 48h post injection of (**B**) NPs and (**C**) PM-NPs. From top to bottom, left to right, 1: brain; 2: heart; 3: spleen; 4: lung; 5: kidney; 6: liver; 7: another kidney; 8: tumor. (**D**) Region-of-interest analysis of fluorescent intensities from major organs and the tumors (**p <0.01). (**E**) The fluorescence images of the tumor slices of 4T1 bearing mice treated with NPs and PM-NPs. Scale bar:100 μm.

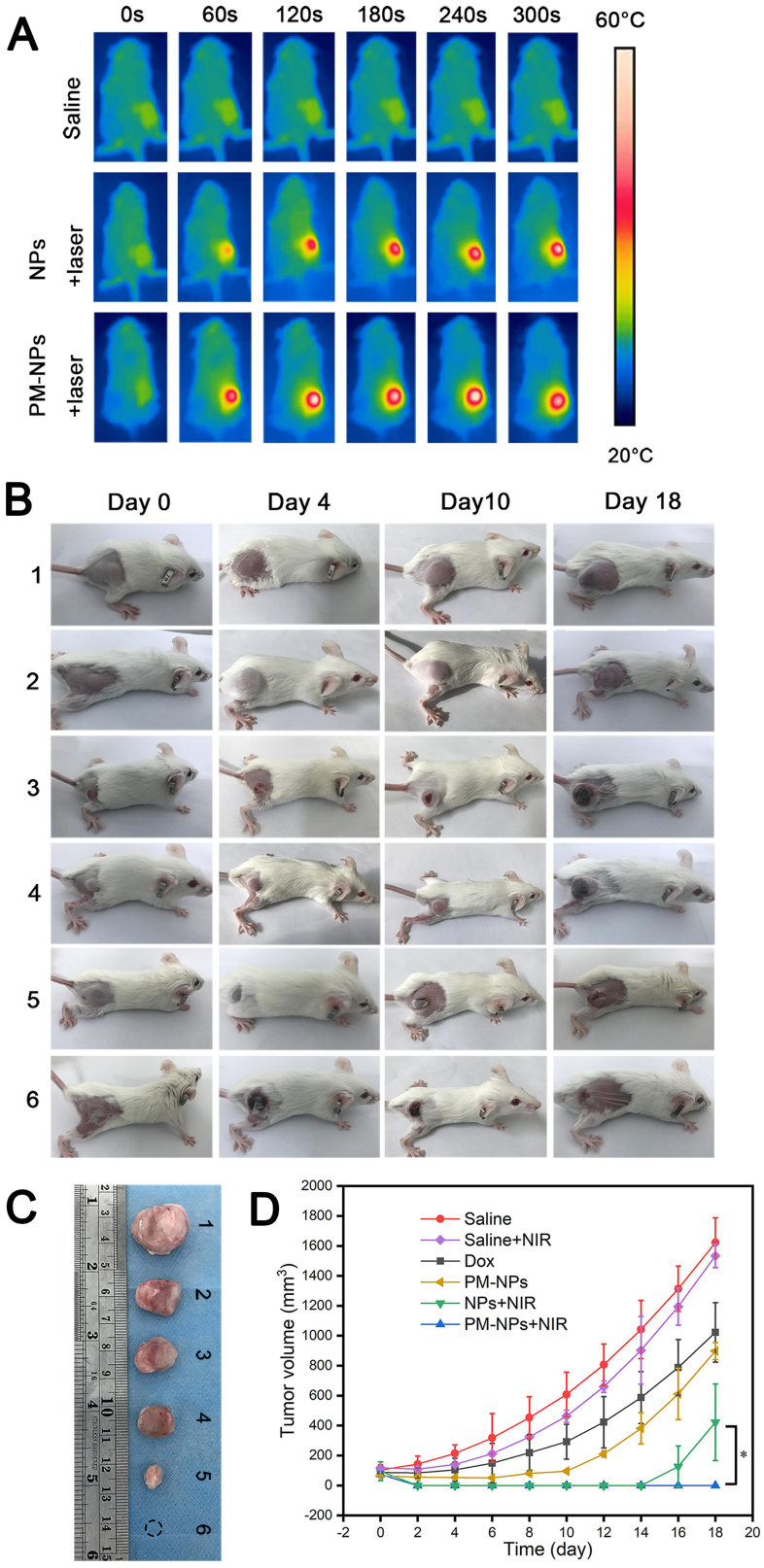

Figure 7 In vivo antitumor effect of PM-NPs. (**A**) Infrared thermal images of tumor-bearing mice treated with saline, and NPs or PM-NPs with laser irradiation (808 nm, 1 W/cm , 5 min). (**B**) Representative digital images of tumor-bearing mice at 0, 4, 10, 18 days after various treatment: (1) saline, (2) saline+ laser, (3) Dox, (4) PM-NPs only, (5) NPs +laser, (6) PM-NPs +laser. (**C**) Representative images of the tumors after different treatment at day 18. (**D**) Tumor growth in tumor-bearing mice by treatment groups. (*p <0.05).

(group 6) (Figure 7C). However, the tumors of the mice treated with the other groups showed a tendency to recur (Figure 7D). Moreover, the body weight of the mice in the NPs group with laser irradiation (group 5) fluctuated significantly compared with that of the mice in saline control group, while the body weight of those mice in the PM-NPs group with laser treatment (group 6) only showed small fluctuations (Figure S6, Supporting Information). Terminally, the mice were sacrificed after 18 days, and their organs were subjected to H&E staining (Figure S7,

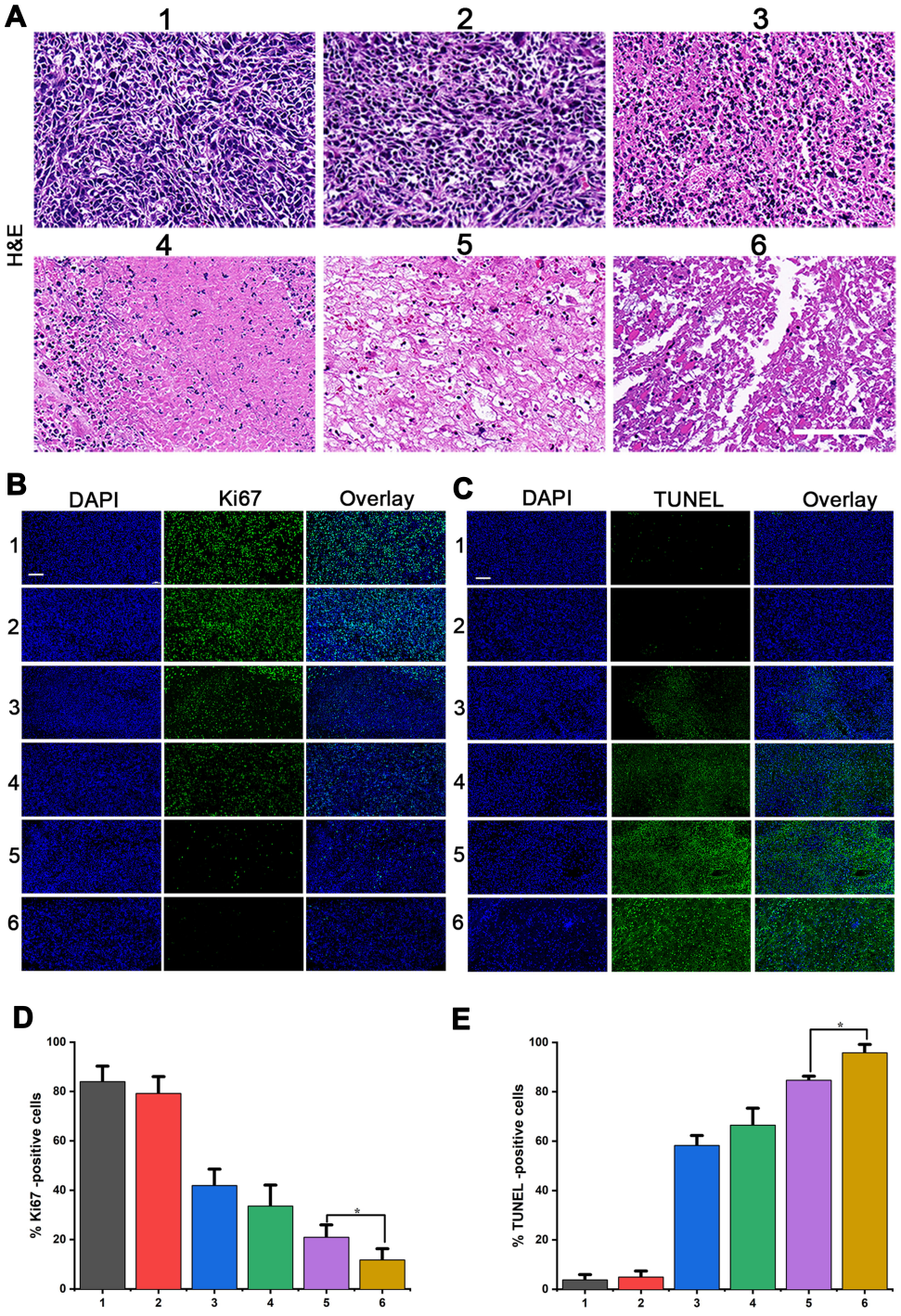

Figure 8 Histological observation and detection of proliferation and apoptosis in the tumor tissues after treatment. The tumor sections were stained with (**A**) hematoxylin and eosin, (**B**) Ki67 for proliferation (green) and DAPI for nuclei (blue), (**C**) TUNEL (green) for apoptosis and DAPI for nuclei (blue). (**D**) Relative Ki67-positive cells and (**E**) TUNEL-positive cells in tumor tissues after different treatments (*p<0.05) The numeric label for each tumor is as follows: (1) saline, (2) saline+ laser, (3) Dox, (4) PM-NPs only, (5) NPs +laser, (6) PM-NPs +laser. Scale bar: 100 μm.

Supporting Information). The results indicated that no obvious damage occurred to the normal tissues, indicating that our nanoplatform was relatively safe.

The in vivo antitumor effect was further investigated via pathological observation. The tumors were collected and preserved with 4% paraformaldehyde, and H&E staining was carried out (Figure 8A). In the saline group with or without laser irradiation (groups 1 and 2), the tumor cells grew vigorously, and abundant blood vessels could be observed. In the Dox group (group 3) and the PM-NPs group (group 4), both of which did not receive laser treatment, apoptotic cells could be observed, but live tumor cells still remained. In group 5 and group 6, the number of dead cells increased, and hollow areas could be observed. The antitumor effect of our nanoparticles was further confirmed by Ki67 and TUNEL immunofluorescence staining (Figure 8B and C). Large areas of apoptotic cells (TUNEL-labeled green fluorescence) were observed in groups 5 and 6, and the number of proliferating cells (Ki-67-labeled green fluorescence) decreased, which was consistent with previous results. As shown in Figure 8D and E, 18.32% of the tumor cells were proliferative, and 95.81% were apoptotic in group 6; 76.68% of TUNEL-positive cells and 22.71% of Ki67-positive cells were apoptotic in group 5, while only 79.28% of Ki67-positive proliferative cells and 3.78% of TUNEL-positive apoptotic tumor cells were apoptotic in the saline group (group 1). Groups treated with Dox only (group 3) or PM-NPs only (group 4) had similar levels of apoptotic cells of approximately 58.25% and 66.45% and proliferative cells of approximately 36.63% and 37.22%, respectively. Compared with groups 5 and 6, the proliferative cell index was significantly lower and the apoptosis cell index was notably higher in group 6 than in group 5, indicating that the NPs coated with PM had a better antitumor efficacy than bare NPs ($p< 0.05$).

Conclusion

In conclusion, we successfully prepared PLGA nanoparticle-coated platelet membranes. The nanoparticles had a suitable size and remained stable in PBS, can release Dox smoother than bare NPs. PM-NPs can actively target to 4T1 cells and escape from Raw 264.7 cells thus enhance the tumor cells killing effect in vitro. Interestingly, we observed that the nanoparticles circulated in the blood of mice for a prolonged time and accumulated at the tumor site due to the behavior of the platelets. The PM-NPs can perfectly eliminate the 4T1 tumor tissues because the high accumulation with local NIR irradiation via EPR effect and automatic targeting. Therefore, PM-NPs is a kind of drug-loaded multifunctional platelet-mimicking nanoparticles. PM-NPs has good stability, superior biocompatibility, longer retention time in the blood, stronger targeting ability, reduced side effects, and excellent tumor killing ability. This PM-NPs can provide ideas for further clinical transformation. Finally, more development of such nanobionic systems in clinical diagnosis and treatment is expected.

Acknowledgments

This project was funded by the National Natural Science Foundation of China (Grant No. 81974267 and 81601883) and Hunan Provincial Health Commission Research Foundation Project (Grant No. B2019166).

Disclosure

All authors have no conflicts of interest to disclose.

References

1. Gao Y, Zhang L, Liu Y, et al. Ce6/Mn 2+ -chelated polydopamine@black-TiO 2 nanoprobes for enhanced synergistic phototherapy and magnetic resonance imaging in 4T1 breast cancer. *Nanoscale*. 2020;12(3):1801–1810. doi:10.1039/C9NR09236F
2. Xu J, Liu Y, Li Y, et al. Precise targeting of POLR2A as a therapeutic strategy for human triple negative breast cancer. *Nat Nanotechnol*. 2019;14(4):388–397. doi:10.1038/s41565-019-0381-6
3. Siegel RL, Miller KD, Jemal A. Cancer statistics, 2016. *CA Cancer J Clin*. 2016;66(1):7–30.
4. Suk JS, Xu Q, Kim N, Hanes J, Ensign LM. PEGylation as a strategy for improving nanoparticle-based drug and gene delivery. *Adv Drug Deliv Rev*. 2016;99(Pt A):28–51. doi:10.1016/j.addr.2015.09.012
5. Jokerst V, Lobovkina TL, Zare N. Nanoparticle PEGylation for imaging and therapy. *Nanomedicine*. 2011;6(4):715–728. doi:10.2217/nnm.11.19
6. Fang RH, Kroll AV, Gao W, Zhang L. Cell Membrane Coating Nanotechnology. *Adv Mater*. 2018;30(23):1706759. doi:10.1002/adma.201706759
7. Hu C-MJ, Zhang L, Aryal S, Cheung C, Fang RH, Zhang L. Erythrocyte membrane-camouflaged polymeric nanoparticles as a biomimetic delivery platform. *Proce Nat Acad Sci*. 2011;108(27):10980–10985. doi:10.1073/pnas.1106634108
8. Kona S, Dong J-F, Liu Y, Tan J, Nguyen KT. Biodegradable nanoparticles mimicking platelet binding as a targeted and controlled drug delivery system. *Int J Pharm*. 2012;423(2):516–524. doi:10.1016/j.ijpharm.2011.11.043
9. Anselmo AC, Modery-Pawlowski CL, Menegatti S, et al. Platelet-like Nanoparticles: mimicking Shape, Flexibility, and Surface Biology of Platelets To Target Vascular Injuries. *ACS Nano*. 2014;8(11):11243–11253. doi:10.1021/nn503732m
10. Su T, Huang K, Ma H, et al. Platelet-Inspired Nanocells for Targeted Heart Repair After Ischemia/Reperfusion Injury. *Adv Funct Mater*. 2019;29(4):1803567. doi:10.1002/adfm.201803567
11. Li M, Li J, Chen J, et al. Platelet Membrane Biomimetic Magnetic Nanocarriers for Targeted Delivery and in Situ Generation of Nitric Oxide in Early Ischemic Stroke. *ACS Nano*. 2020;14(2):2024–2035. doi:10.1021/acsnano.9b08587

12. Song Y, Huang Z, Liu X, et al. Platelet membrane-coated nanoparticle-mediated targeting delivery of Rapamycin blocks atherosclerotic plaque development and stabilizes plaque in apolipoprotein E-deficient (ApoE−/−) mice. *Nanomedicine*. 2019;15(1):13–24. doi:10.1016/j.nano.2018.08.002
13. Li J, Angsantikul P, Liu W, et al. Biomimetic Platelet-Camouflaged Nanorobots for Binding and Isolation of Biological Threats. *Adv Mater*. 2018;30(2):1704800. doi:10.1002/adma.201704800
14. Bernal-Chavez SA, Alcala-Alcala S, Cerecedo D, Ganem-Rondero A. Platelet lysate-loaded PLGA nanoparticles in a thermo-responsive hydrogel intended for the treatment of wounds. *Eur j Pharm Sci*. 2020;146:105231. doi:10.1016/j.ejps.2020.105231
15. He Y, Li R, Liang J, et al. Drug targeting through platelet membrane-coated nanoparticles for the treatment of rheumatoid arthritis. *Nano Res*. 2018;11(11):6086–6101. doi:10.1007/s12274-018-2126-5
16. Owen MR, Byrne HM, Lewis CE. Mathematical modelling of the use of macrophages as vehicles for drug delivery to hypoxic tumour sites. *J Theor Biol*. 2004;226(4):377–391. doi:10.1016/j.jtbi.2003.09.004
17. Mi-Ran Choi KJS-M, Stanley JK, Levin, CS. Rizia Bardhan DA, |Sunil Badve, Jennifer Sturgis, J. Paul Robinson, Rashid Bashir NJH, ‡,§,+ and Susan E. Clare. A Cellular Trojan Horse for Delivery of Therapeutic Nanoparticles into Tumors. *Am Chem Soc*. 2007;7:3759–3765.
18. Dou H, Destache CJ, Morehead JR, et al. Development of a macrophage-based nanoparticle platform for antiretroviral drug delivery. *Blood*. 2006;108(8):2827–2835. doi:10.1182/blood-2006-03-012534
19. Wieczorek A, Uharek L. Genetically modified T cells for the treatment of malignant disease. *Transfusion Med Hemotherapy*. 2013;40(6):388–402. doi:10.1159/000357163
20. Lamers CH, Sleijfer S, van Steenbergen S, et al. Treatment of metastatic renal cell carcinoma with CAIX CAR-engineered T cells: clinical evaluation and management of on-target toxicity. *Mol Ther*. 2013;21(4):904–912. doi:10.1038/mt.2013.17
21. Dafeng Chu D, Gao J, Wang Z. and ZhenjiaWang. Neutrophil-Mediated Delivery of Therapeutic Nanoparticles across Blood Vessel Barrier for Treatment of Inflammation and Infection. *ACS Nano*. 2015;9(12):11800–11811. doi:10.1021/acsnano.5b05583
22. Chu D, Dong X, Shi X, Zhang C, Wang WZ. Neutrophil-Based Drug Delivery Systems. *Adv Mater*. 2018;30(22):1706245. doi:10.1002/adma.201706245
23. Wang W, Xiang C, Mou X. Stem cells as cellular vehicles for gene therapy against glioblastoma. *Int J Clin Exp Med*. 2015;8:17102–17109.
24. Roger M, Clavreul A, Venier-Julienne M-C, et al. Mesenchymal stem cells as cellular vehicles for delivery of nanoparticles to brain tumors. *Biomaterials*. 2010;31(32):8393–8401. doi:10.1016/j.biomaterials.2010.07.048
25. Li L, Guan Y, Liu H. Silica Nanorattle–Doxorubicin-Anchored Mesenchymal Stem Cells for Tumor-Tropic Therapy. *ACS Nano*. 2011;5(9):7462–7470. doi:10.1021/nn202399w
26. Aboody KS, Najbauer J, Danks MK. Erratum: stem and progenitor cell-mediated tumor selective gene therapy. *Gene Ther*. 2008;15(14):1072. doi:10.1038/gt.2008.106
27. Cheng H, Kastrup CJ, Ramanathan R. CJK, R. Ramanathan, D. J. Siegwart, M. Ma, S. R. Bogatyrev, Q. Xu, K. A. Whitehead, R. Langer and D. G. Anderson. Nanoparticulate Cellular Patches for Cell-Mediated Tumoritropic Delivery. *ACS Nano*. 2010;4(2):625–631. doi:10.1021/nn901319y
28. Sun X, Wang C, Gao M, Hu A, Liu Z. Remotely Controlled Red Blood Cell Carriers for Cancer Targeting and Near-Infrared Light-Triggered Drug Release in Combined Photothermal-Chemotherapy. *Adv Funct Mater*. 2015;25(16):2386–2394. doi:10.1002/adfm.201500061
29. Jiang A, Song B, Ji X, et al. Doxorubicin-loaded silicon nanoparticles impregnated into red blood cells featuring bright fluorescence, strong photostability, and lengthened blood residency. *Nano Res*. 2018;11(4):2285–2294. doi:10.1007/s12274-017-1850-6
30. Han X, Wang C, Liu Z. Red Blood Cells as Smart Delivery Systems. *Bioconjug Chem*. 2018;29(4):852–860. doi:10.1021/acs.bioconjchem.7b00758
31. Gao M, Hu A, Sun X, et al. Photosensitizer Decorated Red Blood Cells as an Ultrasensitive Light-Responsive Drug Delivery System. *ACS Appl Mater Interfaces*. 2017;9(7):5855–5863. doi:10.1021/acsami.6b15444
32. Brenner JS, Pan DC, Myerson JW, et al. Red blood cell-hitchhiking boosts delivery of nanocarriers to chosen organs by orders of magnitude. *Nat Commun*. 2018;9(1):1. doi:10.1038/s41467-018-05079-7
33. Shi Q, Montgomery RR. Platelets as delivery systems for disease treatments. *Adv Drug Deliv Rev*. 2010;62(12):1196–1203. doi:10.1016/j.addr.2010.06.007
34. Yang J, Wang S, Liu P. SW, P. Liu, L. Dai, B. Chen, J. Luan and J. Zhou. Platelet-inspired medicine for tumor therapy. *Oncotarget*. 2017;8(70):115748. doi:10.18632/oncotarget.22853
35. Mattias Olsson M, Bruhns P, Frazier WA, Ravetch AJV, Oldenborg P. Platelet homeostasis is regulated by platelet expression of CD47 under normal conditions and in passive immune thrombocytopenia. *BLOOD*. 2005;105(9):3577. doi:10.1182/blood-2004-08-2980
36. Nieswandt B, Watson SP. Platelet-collagen interaction: is GPVI the central receptor? *Blood*. 2003;102(2):449–461. doi:10.1182/blood-2002-12-3882
37. Soler L, Sánchez S. Catalytic nanomotors for environmental monitoring and water remediation. *Nanoscale*. 2014;6(13):7175–7182. doi:10.1039/C4NR01321B
38. Singh VV, Wang J. Nano/micromotors for security/defense applications. A review. *Nanoscale*. 2015;7(46):19377–19389. doi:10.1039/C5NR06254C
39. Li Z, Hu S, Cheng K. Platelets and their biomimetics for regenerative medicine and cancer therapies. *J Mater Chem B*. 2018;6(45):7354–7365. doi:10.1039/C8TB02301H
40. Zhu S, Tian R, Antaris AL, Chen X, Dai DH. Near-Infrared-II Molecular Dyes for Cancer Imaging and Surgery. *Adv Mater*. 2019;31(24):e1900321. doi:10.1002/adma.201900321
41. Leitao MM, de Melo-Diogo D, Alves CG, Lima-Sousa R, Correia IJ. Prototypic Heptamethine Cyanine Incorporating Nanomaterials for Cancer Phototheragnostic. *Adv Healthc Mater*. 2020;9(6):e1901665. doi:10.1002/adhm.201901665
42. Alves CG, Lima-Sousa R, de Melo-diogo D, Louro RO, Correia IJ. IR780 based nanomaterials for cancer imaging and photothermal, photodynamic and combinatorial therapies. *Int J Pharm*. 2018;542(1–2):164–175. doi:10.1016/j.ijpharm.2018.03.020
43. Zhang M, Ye -J-J, Xia Y, et al. Platelet-Mimicking Biotaxis Targeting Vasculature-Disrupted Tumors for Cascade Amplification of Hypoxia-Sensitive Therapy. *ACS Nano*. 2019;13(12):14230–14240. doi:10.1021/acsnano.9b07330
44. Wei X, Gao J, Fang RH, et al. Nanoparticles camouflaged in platelet membrane coating as an antibody decoy for the treatment of immune thrombocytopenia. *Biomaterials*. 2016;111:116–123. doi:10.1016/j.biomaterials.2016.10.003
45. Wang L, Chen SJ, Zhu Y, et al. Triple-Modal Imaging-Guided Chemo-Photothermal Synergistic Therapy for Breast Cancer with Magnetically Targeted Phase-Shifted Nanoparticles. *ACS Appl Mater Inter*. 2018;10(49):42102–42114. doi:10.1021/acsami.8b16323
46. Li J, Ai Y, Wang L, et al. Targeted drug delivery to circulating tumor cells via platelet membrane-functionalized particles. *Biomaterials*. 2016;76:52–65. doi:10.1016/j.biomaterials.2015.10.046
47. Wang L, Chen S, Pei W, Huang B, Niu C. Magnetically targeted erythrocyte membrane coated nanosystem for synergistic photothermal/chemotherapy of cancer. *J Mater Chem B*. 2020;8(18):4132–4142. doi:10.1039/D0TB00364F
48. Zhang M, Wang WT, Wu F, Graveran K, Zhang J, Wu CZ. Black Phosphorus Quantum Dots Gated, Carbon-Coated Fe 3 O 4 Nanocapsules (BPQDs@ss-Fe 3 O 4 @C) with Low Premature Release Could Enable Imaging-Guided Cancer Combination Therapy. *Chem-Eur J*. 2018;24(49):12890–12901. doi:10.1002/chem.201801085

49. Chen S, Huang B, Pei W, et al. Magnetically targeted nanoparticles for imaging-guided photothermal therapy of cancer. *RSC Adv*. 2019;9(65):38154–38164. doi:10.1039/C9RA08281F
50. Kumar P, Treuren TV, Ranjan AP, Chaudhary P, Vishwanatha JK. In vivo imaging and biodistribution of near infrared dye loaded brain-metastatic-breast-cancer-cell-membrane coated polymeric nanoparticles. *Nanotechnology*. 2019;30(26):265101. doi:10.1088/1361-6528/ab0f46
51. Cherukula K, Uthaman S, Park I-K. Design of an Amphiphilic Poly(aspartamide)-mediated Self-assembled Nanoconstruct for Long-Term Tumor Targeting and Bioimaging. *Molecules*. 2019;24(5):885. doi:10.3390/molecules24050885
52. Huang Z, Huang Y, Wang W, et al. Relationship between particle size and lung retention time of intact solid lipid nanoparticle suspensions after pulmonary delivery. *J Control Release*. 2020;325:206–222. doi:10.1016/j.jconrel.2020.06.004